Journal of Coastal Research	30	2	418–428	Coconut Creek, Florida	March 2014

A Coastal Yucatan Sinkhole Records Intense Hurricane Events

Alyson L. Brown[†]*, Eduard G. Reinhardt[†], Peter J. van Hengstum[‡], and Jessica E. Pilarczyk[§]

[†]School of Geography and Earth Sciences
McMaster University
Hamilton, Ontario L8S 4K1, Canada

[‡]Department of Geology and Geophysics
Woods Hole Oceanographic Institution
Woods Hole, MA 02540, U.S.A.

[§]Department of Earth and Environmental Science
University of Pennsylvania
Philadelphia, PA 19104, U.S.A.

www.cerf-jcr.org

www.JCRonline.org

ABSTRACT

Brown, A.L.; Reinhardt, E.G.; van Hengstum, P.J., and Pilarczyk, J.E., 2014. A coastal Yucatan sinkhole records intense hurricane events. *Journal of Coastal Research,* 30(2), 418–428. Coconut Creek (Florida), ISSN 0749-0208.

The potential of tropical sinkholes as archives for historical hurricane events has yet to be fully explored. This study uses high-resolution (1-cm interval) particle-size analysis to examine two sediment push cores from Laguna Chumkopó, located on the Yucatan Peninsula, Mexico. Core CKC1 (62 cm) was collected from the base of a deep sinkhole located in Laguna Chumkopó at –79.9 m (msl), while the second core, CKC2 (93 cm), was collected from the shallow peripheral margin at –6.4 m (msl). Two coarse fining upward sequences (12 to 35 cm, 46 to 62 cm) in CKC1 had mean particle sizes of approximately 1.5 φ (medium sand) with intervening intervals of lime mud (<4 φ). Measured ^{137}Cs activity in the bulk sediment ($n = 15$) and radiocarbon dating ($n = 3$) using bomb-carbon calibration determined that the lower coarse unit was deposited in the 1960s (after September 1957 AD), and the upper unit between January 1985 and August 1991 AD. Hurricane Gilbert struck the Yucatan on 15 September 1988 as a category 5 storm, generating the upper fining upward sequence. Hurricane Beulah (category 2–3) likely generated the lower unit when it struck on 18 September 1967. CKC2 revealed small textural changes, alternating between silt and sand-sized particles and radiocarbon ages dated to ~6.7 to 7.1 ka. The rapid accumulation of sediment in the shallow lagoon likely occurred with rising sea level flooding the area at approximately 6.8 ka. Based on the sedimentary results, a depositional model is proposed for inland sinkholes, explaining the formation of hurricane deposits through density and debris flows along the shallow margin.

ADDITIONAL INDEX WORDS: *Sediment, depositional model, particle size analysis, sinkhole, hurricanes.*

INTRODUCTION

Tropical cyclones represent a global threat to coastal environments and resources because they destroy landforms, ecosystems, infrastructure, and cause loss of human life. It has been proposed that tropical cyclone intensity (≥category 3 on the Saffir-Simpson Scale, used hereafter) and tropical cyclone frequency have increased during the short instrumental record (Nyberg *et al.,* 2007; Webster *et al.,* 2005) and will increase with global warming (Knutson *et al.,* 2010; Webster *et al.,* 2005). Sedimentary records documenting past tropical cyclones represent an important archive for determining how a warming climate will modulate tropical cyclone activity.

A widely applied technique for reconstructing tropical cyclone activity uses sandy overwash deposits that accumulate in quiescent coastal basins. Tropical cyclones cause storm surges up to several meters that overwash coastal landforms (*e.g.*, beach barriers) entraining and depositing coarse-grained sediment in basins that normally have fine-grained background sedimentation. Salt marshes are frequently used for reconstructing hurricane activity (Boldt *et al.,* 2010; Donnelly *et al.,* 2001; Horton, Rossi, and Hawkes, 2009; Nyman, Crozier, and DeLaune, 1995; Parsons, 1998; Reese *et al.,* 2008), but overwash deposits are also found in coastal lagoons, lakes, and mangroves (*e.g.*, Castañeda-Moya *et al.,* 2010; Donnelly and Woodruff, 2007; Liu and Fearn, 1993, 2000). Although these environments have been useful, they do have limitations. Existing coastal environments typically do not contain events older than 5–6 ka as most of them formed during decelerating sea-level rise in the mid-Holocene, and overwash records may be incomplete because of erosion and non-deposition during successive storms or hurricanes. The long-term stability of the barriers and the formation of lagoons may also be a factor, as they may migrate with rising sea level or changing wave climate.

Coastal karst basins (CKBs) have received little attention as hurricane recorders. CKBs include a variety of karst features formed by carbonate dissolution and modification, such as sinkholes (cenotes), blueholes, or underwater caves (van Hengstum *et al.,* 2011). CKBs are often flooded with the coastal aquifer because of high porosity of the limestone terrain, and the water level often reflects the sea level oscillating over glacioeustatic cycles (Shinn *et al.,* 1996; Surić *et al.,* 2005; van Hengstum *et al.,* 2011). As such, sinkholes deeper than 80 m have been flooded since the early Holocene and may have long sedimentary sequences (Dill *et al.,* 1988; Gischler and Hudson, 2004; Shinn *et al.,* 1996). CKB morphology is also relatively static (*e.g.*, limestone bedrock), which makes it an ideal sediment trap with minimal erosion and re-deposition, unlike transient sand barriers in estuarine settings (Shinn *et al.,* 1996).

DOI: 10.2112/JCOASTRES-D-13-00069.1 received 22 March 2013; accepted in revision 2 July 2013; corrected proofs received 15 October 2013.
Published Pre-print online 5 December 2013.
*Corresponding author: browna22@mcmaster.ca

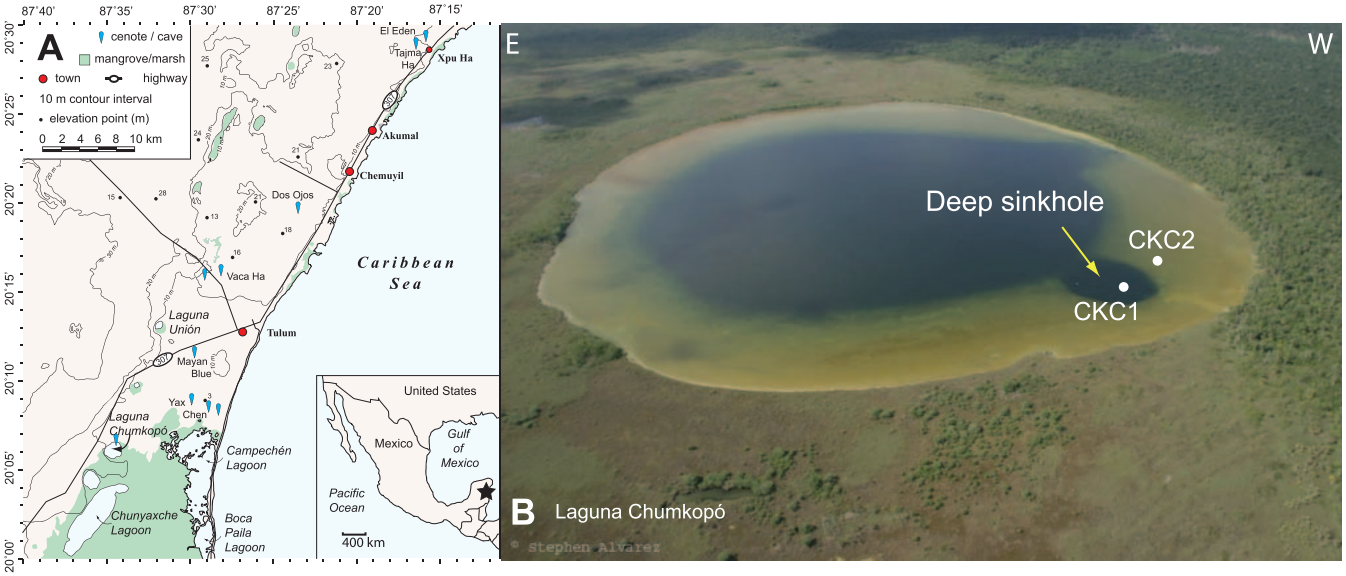

Figure 1. (A) Map of the Caribbean (inset) and regional topography on the eastern coast of the Yucatan Peninsula. (B) Aerial photograph (looking south) of Laguna Chumkopó detailing location of CKC1 and CKC2 (photo provided by Stephen Alvarez). (Color for this figure is available in the online version of this paper.)

Few studies have examined the sediments in CKBs from a paleotempestology perspective. Gischler *et al.* (2008) examined sediment cores (up to 6 m long) from Blue Hole, Belize, which contained carbonate mud interrupted by several (*e.g.*, $n = 39$, Core 2) coarse-grained hurricane overwash units with a sediment accumulation rate of 2.5 mm y^{-1}. The Blue Hole is found on Lighthouse Reef approximately 80 km offshore and has a water depth of ~120 m. Recently, Lane *et al.* (2011) presented a decadal paleohurricane record (6 m in length) from Mullet Pond in NW Florida. Mullet Pond is a 200 m diameter sinkhole mostly infilled with sediment (sand, peat, and muds). The pond is 350 m from Apalachee Bay with a water depth of ~1.5 m and is separated from the bay by a 3 to 4 m high dune ridge. The sinkhole is located 100 m inland and has a sedimentation accumulation rate varying between 1.3 to 1.8 mm y^{-1}.

These two studies demonstrate that CKBs are sensitive to hurricane sedimentation; however, they are located within the coastal zone with different geomorphology compared to inland karst basins. Great Blue Hole, Belize, is a very deep basin in an offshore reef setting infilled with detrital carbonates, whereas Mullet Pond is shallow, in the coastal zone, and largely filled with clastic and organic sediments. Inland karst basins have not been used for hurricane records even though low-lying terrestrial areas on tropical and subtropical carbonate platforms contain numerous sinkholes. Studies from Little Salt Spring, ~20 km from the coast in SW Florida and at 72 m water depth show long accumulation histories spanning the last ~13.5 ka (Alvarez Zarikian *et al.,* 2005; Bernhardt *et al.,* 2010). Coarse layers were noted, but the focus was paleoclimatic rather than reconstructing storm deposition. Intrinsically, inland sinkholes would respond differently to hurricanes than those on the coast or continental shelf (*e.g.*, overwash), but there is no research examining whether inland sinkholes can preserve hurricane records. Therefore, the objective of this study is to test the sensitivity of an inland sinkhole to hurricane sedimentation and provide a depositional model for future applications.

STUDY AREA

Laguna Chumkopó is a shallow basin located 10 km inland of the Caribbean coast on the Yucatan Peninsula, Mexico, and is approximately 4 km east of the large Campechén Lagoon (20°9.752′ N, 87°33.230′ W; Figure 1). The surficial geology consists of heavily karstified Pliocene to upper Miocene-aged limestones that are less than 5 m above mean sea level (msl; Beddows, 2004; Smart *et al.,* 2006; Weidie, 1985). It is surrounded by tropical arid forest and has mixed marshlands (*e.g.*, mangroves, cattails; Figure 2A) fringing its periphery (Meacham, 2012). Despite regional topographic variations, the water level of Chumkopó is close to msl (~10 cm) because the hydraulic gradient across the Yucatan is low at ~0.5 to 1.0 cm km^{-1} (Beddows, 2004).

Laguna Chumkopó consists of a large basin with a surface area of ~384 m^2, with a water depth of approximately 15 m that shoals to ~7 m around the periphery. A smaller, deeper sinkhole (–80 m [msl]) approximately 65 m in diameter is located on the northern side of Chumkopó that creates a secondary depocenter. Based on diver surveys (Figure 2B,C), the sinkhole has a bell-like geometry with limestone overhangs and a relatively flat sedimentary bottom with no associated cave passage. This physiography is similar to shaft-style blue holes found in the Bahamas (Mylroie, Carew, and Moore, 1995;

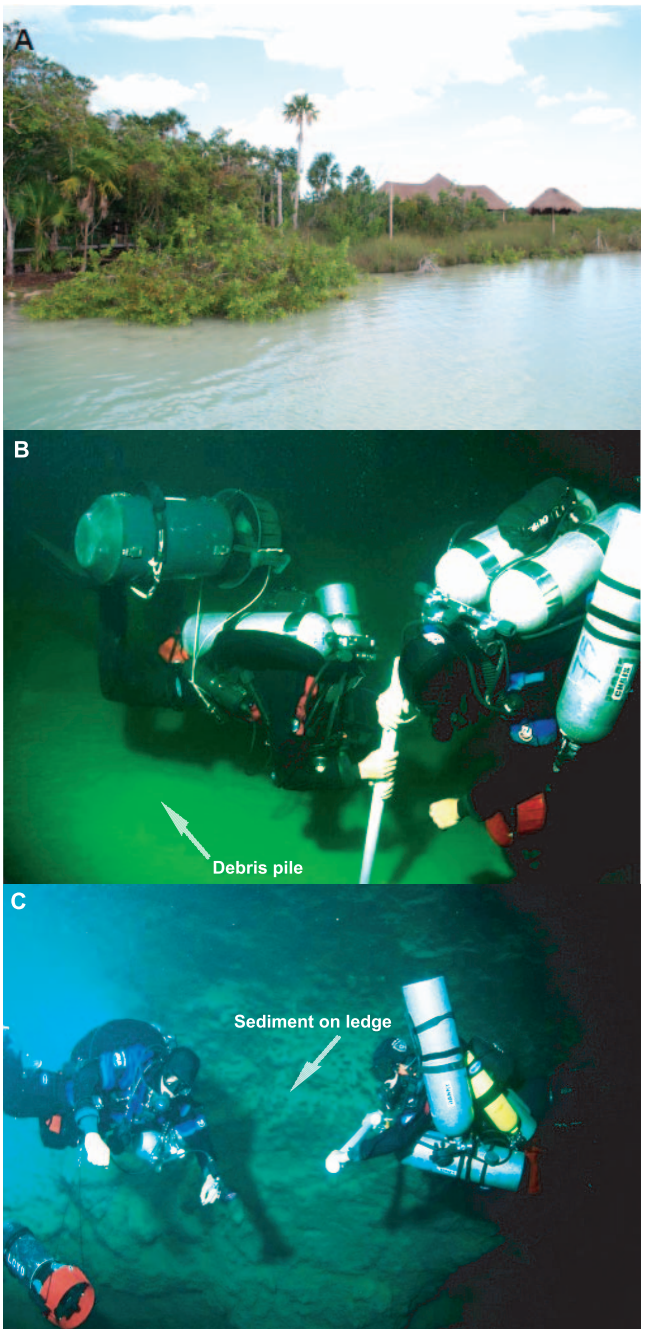

Figure 2. (A) Photograph looking south showing the transition from tropical arid forest and mixed mangrove/marsh. (B) Divers taking core on bottom of sinkhole; note the debris pile (see "Discussion" for details [photo provided by David Rhea]). (C) Divers decompressing at ledge on the side of the sinkhole; note the sediment on ledge (photo provided by David Rhea). (Color for this figure is available in the online version of this paper.)

Steadman *et al.,* 2007), suggesting a similar polygenetic origin for the sinkhole in Laguna Chumkopó. Vertical outcrops of lime muds with variable amounts of shells surround the periphery of the sinkhole. Hydrogeologically, the sinkhole is flooded by stratified groundwater with a thick (≈1 m) H_2S layer and a sharp transition in salinity, oxygen, and temperature at –22 m (msl; Figure 3). This stratification typifies the groundwater structure of many anchialine systems in CKBs on the eastern Yucatan Peninsula (Beddows, 2004, 2005; Beddows *et al.,* 2007) and worldwide (*e.g.*, Schwabe and Herbert, 2004; Steadman *et al.,* 2007; van Hengstum and Scott, 2012).

Most hurricanes that approach the Yucatan Peninsula originate in the Main Development Region (between 9° N and 21.5° N; Figure 4) in either the tropical Atlantic or western Caribbean Sea. The instrumental record documents a total of 107 storms striking the Yucatan (NOAA, 2010; Figure 4) between 1851 to 2000; 73% of the hurricane strikes were weaker storms (category 1 and 2 events), and 27% were intense hurricane events (≥category 3 events; Boose *et al.,* 2003). Of all the storms to strike the Yucatan, only 12 events have hit within a 75 km radius of Chumkopó, and only three events are classified as intense hurricanes: (1) Hurricane Charlie hit as a category 4 event in August 1951; (2) Hurricane Gilbert hit as a category 5 event in 1988; and (3) Hurricane Emily hit as a category 4 event in 2005 (NOAA, 2011). Hurricane Roxanne was a moderately intense event because it briefly achieved category 3 status ~65 km offshore (maximum wind speed of 51.4 m s^{-1}) on 11 October 1995 but weakened rapidly and likely hit the coast as a category 2 event (wind speed <48 m s^{-1}). Of all the intense hurricanes to strike the Yucatan, Hurricane Gilbert was one of the most destructive. Gilbert made landfall as a category 5 event over Cozumel, Mexico, at 1400 UTC 14 September 1988, with winds at or above 297.7 km h^{-1} and caused a storm surge between 2–4 m. Gilbert caused 202 deaths in Mexico and $1–2 billion in damage (NOAA, 2010). The weak hurricane events (categories 1 and 2) making landfall within 75 km of Chumkopó are more numerous (1879, 1887, 1922, 1933, 1938, 1944, 1955, and 1995) with Hurricane Beulah in 1967 (category 2) following an almost identical geographic track across the Yucatan Peninsula as Hurricane Gilbert.

METHODS

Two short push cores were collected by SCUBA divers in 2008 to determine if Laguna Chumkopó was a hurricane recorder: one was collected from the shallow periphery of the primary basin (CKC2: 20°9.883′ N, 87°33.214′ W) and another from the bottom of the sinkhole (CKC1: 20°9.904′ N, 87°33.179′ W). Sediment cores were extruded, described (color, general texture, sedimentary structures, *etc.*), photographed, and subsampled at 1-cm intervals for transport back to the laboratory. Water-mass conditions were measured using a HydroLab water quality MS5 multiprobe; temperature (±0.10 °C), dissolved oxygen (±0.01 mg/L for 0–8 mg/L; ±0.02 mg/L for >8 mg/L), redox (±20 mV), pH (±0.2 units), specific conductivity (±1% of reading; ±0.001 mS/cm), and salinity (±0.2 ppt).

Textural analysis of bulk sediment samples (cm scale) was conducted using a Beckman-Coulter LS 230 particle-size analyzer using the Fraunhofer optical model. Particle size distributions (PSDs) were log transformed to the phi-scale, interpolated using a krigging algorithm, and graphed as a color surface plot (Beierle *et al.,* 2002; Donato *et al.,* 2009; Reinhardt, Nairn, and Lopez, 2010; van Hengstum *et al.,* 2007, 2011). Loss

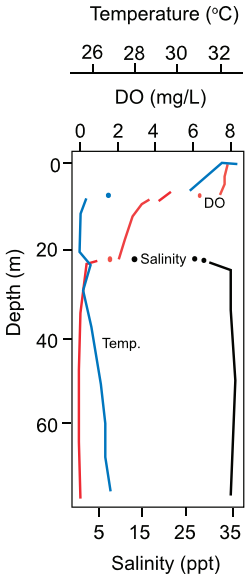

Figure 3. Hydrographic conditions in Cenote Chumkopó measured on 2 October 2009. (Color for this figure is available in the online version of this paper.)

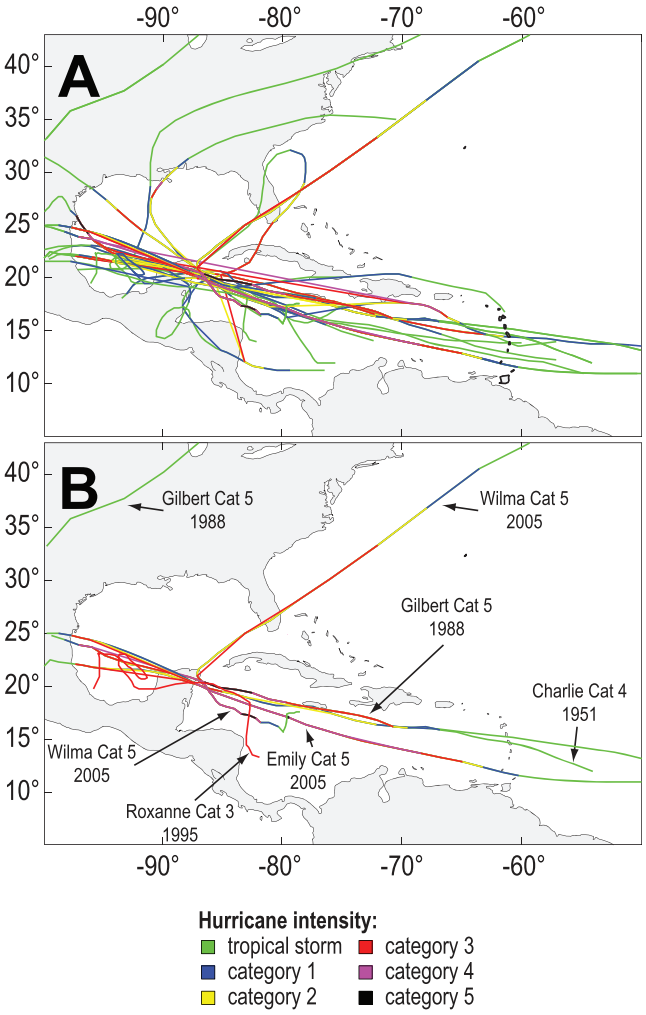

Figure 4. (A) Instrumental record of hurricane events within a 120-km radius of Cenote Chumkopó, Mexico. (B) Storm tracks of the six most intense hurricanes (≥category 3 on the Saffir-Simpson scale), labeled according to maximum strength achieved by each storm. (Color for this figure is available in the online version of this paper.)

on ignition analysis followed Heiri, Lotter, and Lemcke (2001) to determine bulk organic-matter (OM) content in the sediment. Samples were dried in an oven at 105 °C for 12 h to remove moisture followed by ignition at 550 °C for 2–3 h in a Fisher Isotemp® 550 Series Muffle Furnace (model number 550-58). OM content was calculated as weight percent (%). Sand content (g/cm^3) was calculated by weighing dry sediment (2.5 cm^3) before and after sieving with a 63-μm mesh.

Core chronologies used seven accelerator mass spectrometry radiocarbon (^{14}C) ages (Beta Analytic), and ^{137}Cs activity in the bulk sediment measured in a Canberra GL2020s low-energy germanium gamma well detector (n = 15). Terrestrial OM (leaves, twigs) was used for radiocarbon dating, as there are large hard-water effects with shells as reported from a previous study (Gabriel *et al.,* 2009). Dated OM had $^{\text{TM}}\delta^{13}C_{org}$ values reflecting terrestrial C_4 plant origins (Gabriel *et al.,* 2009; Lamb, Wilson, and Leng, 2006). Conventional radiocarbon ages containing a fraction ($F^{14}C$) exceeding 1.0000 postdate 1950 AD (Reimer *et al.,* 2004) were calibrated with CALIbomb using the Northern Hemisphere Zone 2 atmospheric ^{14}C calibration curve that has a sub-annual resolution (Blaauw, 2010; Hua and Barbetti, 2004; Marshall *et al.,* 2007). Dates with a fraction modern less than 1.0000 were calibrated using IntCal09 (Reimer *et al.,* 2009; Blaauw, 2010).

^{137}Cs activity was measured in 1-cm intervals downcore to define the 1963 AD chronohorizon in the stratigraphic record (*e.g.*, Donnelly and Woodruff, 2007; Lane *et al.,* 2011; Reinhardt, Nairn, and Lopez, 2010). Because ^{137}Cs is a man-made radionuclide, the onset and peak of ^{137}Cs activity in sedimentary profiles is related to the initiation of nuclear weapons testing in 1954 AD and maximum atmospheric ^{137}Cs levels at 1963 AD prior to the nuclear weapons moratorium (Pennington, Cambray, and Fisher, 1973; Ritchie and McHenry, 1990).

RESULTS

Hydrography

Chumkopó's hydrological conditions typify those found throughout the Yucatan Peninsula, where an upper meteoric lens (1.11 ppt, low oligohaline) rests on top saline groundwater intruding from the ocean (36.48 ppt; Beddows *et al.,* 2007; Moore, Stoessell, and Easley, 1992; Whitaker and Smart, 1990). The water masses, as measured in the sinkhole, show a halocline (or 53-cm mixing zone) dividing the upper meteoric lens from the basal saline groundwater at –22.37 to –22.9 m (msl; Figure 3). Oxic conditions are found in the meteoric lens (*e.g.*, 8.03 mg L^{-1} at 0.06 m), while dysoxic to anoxic conditions

characterize the basal saline water mass (*e.g.*, 0.02 mg L^{-1} at –35.57 m [msl]).

The thermal profile is more complex and likely reflects a combination of seasonal and annual groundwater processes. The meteoric lens is thermally divided, with an upper layer from 0 to –6.9 m (msl) that decreases in temperature from 32.7 to 30.4 °C, followed by a sharp thermocline and relatively stable temperatures (25.4 to 25.6 °C) from –6.9 to –22.7 m (msl). From –22.7 m (msl; halocline), the saline groundwater shows a slowly increasing temperature from 25.6 to 26.9 °C to the base of the sinkhole at –70.9 m (msl; Figure 3). Considering that the hydrographic profile was measured after peak summer insolation in September 2008, the warmer surface layer likely represents seasonal heliothermic heating with high dissolved oxygen values from increased algal productivity. The small temperature increase (<0.5 °C) just below the halocline at –22.9 m (msl; Figure 3) is probably from the landward movement of ocean water at the top of the saline groundwater layer, while increasing temperature with depth may be attributable to geothermal heating (Beddows *et al.,* 2007; Moore, Stoessell, and Easley, 1992).

Chronology

Radiocarbon dates from CKC1 (Table 1) contain more ^{14}C than the modern reference standard and postdate nuclear weapons testing in the 1950s, a result confirmed by the ^{137}Cs activity downcore (Figure 5). The ^{14}C age at the base of CKC1 (61 cm) is January 1956 to August 1957 AD, and the ages at 29 cm and 19 cm are January 1987 to August 1991 AD and January 1985 to January 1989 AD. The core has an average sedimentation rate of ~1.2 cm y^{-1}, which does not consider the effects of rapid event-driven sedimentation. If coarse sedimentary layers are ignored, the background sedimentation rate for the fine-grained interval from 0–12 cm and 35–46 cm is ~0.4 cm yr^{-1}.

The ^{137}Cs activity in the bulk sediment confirms that CKC1 spans the last 50 years. The peak in ^{137}Cs activity occurs from 42–59 cm and reflects the 1963 AD chronohorizon. Given the uncertainties in the measurements, determining the 1963 AD interval is difficult because ^{137}Cs activity does not reach background levels at the bottom of the core; therefore, a typical Cs peak is not displayed. The lower ^{137}Cs activities occurring from 42–59 cm are likely attributable to inputs of older sediments that have no ^{137}Cs activity (discussed subsequently). However, the Cs results do confirm the ^{14}C ages, which indicate that the entire CKC1 succession postdates the onset of atmospheric rainout in 1954 AD.

Radiocarbon dates from CKC2 (Table 1) are significantly older with a basal age at 7.1 ka and an upper date of ~ 6.9 ka at 39 cm. These dates indicate that the majority of the core, ~50 cm, was deposited within ~200 years. Assuming a constant sedimentation rate between the radiocarbon dates (39–91 cm), the average sedimentation rate is 0.25 cm y^{-1}. Sedimentation for the upper section (0–39 cm) of the core shows a considerable reduced rate estimated at $\sim 5.7 \times 10^{-3}$ cm y^{-1}

CKC1 Sedimentology

CKC1 was collected from the deep (–79.85 m) sinkhole in Chumkopó. The core penetrated 127 cm into the sediment, but the final length was 62 cm because of compaction. In general, the sediments in CKC1 (Figure 5) alternated between a light gray, fine-grained carbonate mud (0 to 12 cm, 35 to 46 cm) with two prominent coarse units slightly pinkish in hue (12 to 35 cm, 46 to 62 cm). The mean particle size for the fine-grained units is ~10 φ (clay sized); they contained 5 to 6% OM with low sand contents (~30 g cm^{-3}) and no gastropod shells. Occasional small pebbles (<1.5 cm diameter) were recovered in the topmost section of the core (0 to 18 cm). The PSD plot shows peaked distributions with fine skewing for the fine-grained units. Occasional intact leaves are found, suggesting negligible post-depositional disturbance through bioturbation or re-sedimentation by hydrographic currents.

The prominent coarse-grained units that fined upward in CKC1 contained numerous pebbles and gastropod shells (*Pyrgophoros* sp.) that were also found in the shallow basin sediments documented in core CKC2 (Figure 5). The mean particle-size peaks at 1.5 φ (medium sand), and the sand content exceeds 90 g cm^{-3}. The mode for the two units is ~4.5 φ (coarse silt) but varies from –0.4 φ (very coarse sand) to 6.0 φ (medium silt). The PSD plot shows that the coarse units are less peaked compared to the fine muddy units and that they contain multiple thin mud interbeds. OM contents decrease in the coarse-grained units to a low of ~3%, which also corresponds with increasing sand content (Figure 5). The upper unit displays a gradual fining upward sequence in the mean particle size from 10–22 cm, while in the lower unit the fining is sharper ranging from 47–51 cm, although total sand contents decrease gradually in both cases (Figure 5).

CKC2 Sedimentology

CKC2 was obtained from the shallow margin of Chumkopó from –6.4 m (msl). The initial core length was 103 cm but was reduced to 96 cm after compaction. Overall, CKC2 (Figure 5) is composed of fine-grained, light brown mud (~5 φ, coarse silt) with coarse (~2.75 φ, fine sand) interbeds (~3–4 cm) but records only subtle textural differences compared to CKC1. Sand content within the core is fairly low and varies little, with the highest concentration at ~40 g cm^{-3} in the top 10 cm of the core. The PSD plot shows high peakedness for the muddy intervals with fine-grained skewness, whereas the coarser layers have broader PSDs. OM-rich laminations are found throughout the length of the core, indicating little reworking or disturbance of the sediments since deposition. OM content for the upper portion (0–64 cm) of the core is low at ~3%, and the highest concentration is between 86 and 87 cm (~11%). Both whole and fragmented gastropods are found throughout the succession.

DISCUSSION

Sea-Level Rise and the Flooding of Chumkopó: CKC2

The rising Holocene sea level flooded many sinkholes and caves on the Yucatan Peninsula, which culminated in the mid-Holocene when sea-level rise began decelerating. Gabriel *et al.* (2009) found in Cenote Aktun Ha that by ~6.8 ka, sea-level rise had flooded the sinkhole creating a marsh/mangrove on the central breakdown pile, which is at ~4 m below msl. Initially, sedimentation rates were high (0.65 cm y^{-1}) as sea-level rise flooded the breakdown pile, but by ~6.6 ka, rising sea level had

Table 1. *Radiocarbon results for CKC1 and CKC2. Numbers in bold text refer to dates that have the highest probability.*

Index No.	Lab Number	Core	Core Interval	Material	Conventional ^{14}C Age	Fraction Modern	δ^{13}C (‰)	Calibrated 2σ Ranges	Probability	Calibrated Age
1	Beta - 270687	CKC1	19–20 cm	leaf	–	1.187 ± 0.006	–27.1	1958.21 (Mar) to 1958.90 (Nov)	0.109	
								1985.80 (Oct) to 1989.43 (Jun)	**0.891**	Oct 1985 to Jun 1989
2	Beta - 270688	CKC1	28–29 cm	bulk organics	–	1.117 ± 0.006	–28.5	1958.00 (Jan) to 1958.48 (Jun)	0.086	
								1987.11 (Feb) to 1987.24 (Mar)	0.010	
								1987.88 (Nov) to 1988.45 (Jun)	0.042	
								1988.66 (Aug) to 1990.97 (Dec)	**0.839**	Aug 1988 to Dec 1990
								1991.51 (Jul) to 1991.70 (Sep)	0.023	
3	Beta - 270689	CKC1	61–62 cm	leaf	–	1.069 ± 0.005	–29.6	**1955.97 (Dec) to 1957.53 (Jul)**	**1.000**	Dec 1955 to Jul 1957
4	Beta - 270690	CKC2	39–40 cm	leaf	6030 ± 40	N/A	–25.6	6754 to 6763	0.013	
								6778 to 6982	**0.987**	6880 ± 100 y BP
5	Beta - 270691	CKC2	64–65 cm	bulk organics	6290 ± 40	N/A	–27.5	7034 to 7036	0.002	
								7157 to 7316	**0.998**	7240 ± 80 y BP
6	Beta - 270692	CKC2	76–77 cm	leaf	6090 ± 40	N/A	–25.5	6802 to 6814	0.014	
								6848 to 7030	**0.836**	6940 ± 90 y BP
								7043 to 7070	0.027	
								7077 to 7086	0.009	
								7096 to 7156	**0.113**	7130 ± 30 y BP
7	Beta - 270693	CKC2	90–91 cm	twig	6160 ± 40	N/A	–28.3	**6948 to 7165**	**1.000**	7060 ± 110 y BP

† Beta Analytic sample number.
* Reimer *et al.*, 2004.
‡ Reimer *et al.*, 2009.

drowned the marsh creating open water conditions with low sedimentation rates ($\sim 1.9 \times 10^{-3}$ cm y^{-1}; Gabriel *et al.,* 2009).

The radiocarbon dates from CKC2 indicate that Chumkopó broadly conforms to this regional flooding and sedimentary history. The base of the core has higher OM content (>8%), which is perhaps indicative of increased marshy conditions around the periphery of Chumkopó during initial flooding. Scarps exposed on the sides of the sinkhole contain thin (1–3 cm) peat deposits on basal limestone and at equivalent depth (~8 m) to the OM at the base of CKC2. Sedimentation in Chumkopó began between 6.9 to 7.2 ka (92 cm), accumulated quickly based on the radiocarbon date at 40 cm (6.8–6.9 ka), and is similar to Cenote Aktun Ha. Optimal conditions for calcareous mud production existed during the initial flooding at ~7 ka and may have been biologically mediated (Robbins, Tao, and Evans, 1997; Wright and Burchette, 1996). Reversals in radiocarbon dates in CKC2 suggest sediment reworking along the periphery of Chumkopó, likely caused by increased wave action during storms or hurricanes. No OM was available for radiocarbon dating in the top of the core, but the top 15 cm may represent sedimentation over the last ~6 ka, with the sandier intervals from successive resuspension events during storms and hurricanes in an otherwise low sedimentation environment.

Hurricane Deposits in Chumkopó: CKC1

Sedimentation rates are much higher in the deep sinkhole basin, with 60 cm of sedimentation since 1956 AD (average rate of 1.2 cm y^{-1}). Sediment is not authigenic from primary production but rather originates from resuspension of older sediments in the surrounding shallow areas of Chumkopó during storms and hurricanes. Two coarse-grained intervals, which fine upward in CKC1 at 12–35 cm and 46–62 cm, correlate with hurricane events in the instrumental record. The upper unit is associated with Hurricane Gilbert in 1988 AD, and the lower unit likely originates from Hurricane Beulah in 1967 AD.

The upper coarse-grained interval is dated from January 1985 to August 1991 AD based on two radiocarbon dates that bracket the timing of Hurricane Gilbert, a category 5 storm that hit the Yucatan Peninsula on 14 September 1988 and made landfall <62 km away from Chumkopó. The radiocarbon date from the lower coarse-grained interval provides an age of January 1956 to August 1957 AD, and the ^{137}Cs peak at ~45–60 cm constrains the 1963 AD chronohorizon (Figure 5). The only hurricane to strike within 65 km of Chumkopó after 1963 is Hurricane Beulah in 1967 AD, which struck the Yucatan coast as a category 2 storm with wind speeds of ~46 m s^{-1} (NOAA, 2011) and is a likely candidate for the lower fining upward sequence.

Hurricane Gilbert was both unique in its meteorological structure and devastation to the Yucatan coast. The central eye in most hurricanes is relatively calm, typically measuring ~40 km in diameter, and is surrounded by a wall of thunderclouds referred to as the eye wall (Monarstersky, 1988). The eye wall of the storm contains rain and the strongest winds within the storm (Monarstersky, 1988). Hurricane Gilbert was unique by developing a double eye wall (Monarstersky, 1988). The second, or outer eye wall (~24 km in diameter), formed concentrically

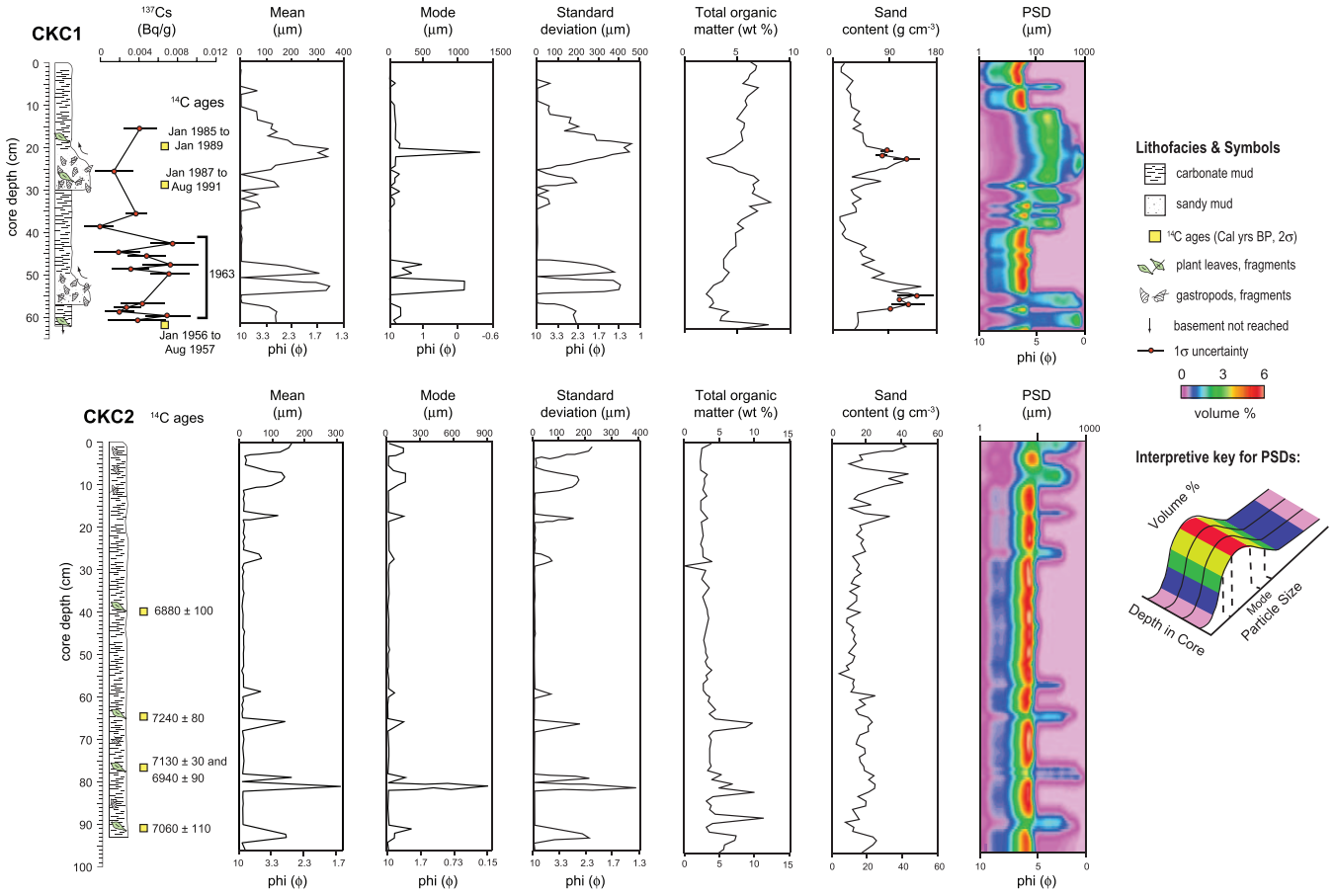

Figure 5. Core lithologies, standard particle-size statistics (mean, mode, and standard deviation), organic matter and sand content, radiocarbon ages, ^{137}Cs activity, and interpolated particle-size distributions (PSDs) for CKC1 and CKC2. The mean value and uncertainty on replicate analysis of the sand content is provided for the coarse-grained units. (Color for this figure is available in the online version of this paper.)

around the inner eye wall (~14.5 km in diameter). The size of the eye of the storm is inversely proportional to the magnitude of the storm; the smaller the eye the greater the wind speed and intensity of the storm. Hurricane Gilbert reached great wind speeds of 297.7 km h^{-1} (NOAA, 2010). Hurricane Gilbert claimed 202 lives in Mexico, causing $1.8 to 3.6 billion in damages, and is the most devastating storm to ever hit the Yucatan in the historical record (NOAA, 2010). Diez, Esteban, and Paz (2009) found that Gilbert was more destructive to the beaches of the Cancun-Nizuc littoral barrier when compared to other hurricanes from its sheer force and extension, including Hurricane Wilma (2005, category 4, landfall ~100 km north of Chumkopó) and Hurricane Roxanne (1995, category 3, landfall <18 km away from Chumkopó). Hurricane Gilbert made landfall considerably closer to Chumkopó than the Cancun-Nizuc beach barrier system. Aside from the magnitude of Hurricane Gilbert, the path of the hurricane helped contribute to its devastating impact. The hurricane maintained a straight path for over 4500 km with only a 5-km divergence, which is rare for large storms (Meyer-Arendt, 1991). Lastly, Hurricane Gilbert generated a storm surge along the eastern coast of Mexico that was reported to be ~2.4 to 4.0 m (NOAA, 2010).

Hurricane Beulah is well known for its impact on the Texas coast with flooding and a record number of tornados (NOAA, 2010). Hurricane Beulah is the only large hurricane that occurred in 1967, and it tracked through the Caribbean Sea hitting the Yucatan Peninsula on 17 September near Cozumel as a category 2 storm with 160 km h^{-1} winds (NOAA, 2010). As it crossed the Yucatan, it caused widespread destruction, roads were flooded, communication lines were cut, agricultural fields were destroyed, and there were 11 fatalities. The hurricane then weakened before moving into the NW Gulf of Mexico, reintensifying to a category 5 and hitting the Texas coast. It created 95 tornadoes, which is the highest number of tornadoes produced by a tropical cyclone, and rains that caused extensive flooding (NOAA, 2010). The geographic pathway traveled by Hurricane Beulah was nearly identical (parallel) to the pathway traveled by Hurricane Gilbert several years later, a factor reasoned by Meyer-Arendt (1991) as contributing to the devastating impact of Hurricane Gilbert.

Hurricane-Induced Sedimentary Processes

Chumkopó is not responding to hurricanes like the classic hurricane-induced overwash of beach-barrier systems (*e.g.*, Donnelly *et al.,* 2001; Morton and Sallenger, 2003). As previously discussed, the stratigraphy at CKC2 indicates that modern sediment production in Chumkopó is quite low, so modern sedimentary processes are dominated by resuspension and reworking of older mid-Holocene sediments. The deep sinkhole acts as a secondary depocenter, where these reworked mid-Holocene sediments settle out of suspension below wave base and eventually to the bottom of the sinkhole. As a hurricane approaches the Yucatan coastline, storm surge may cause a relative increase in water level in the lagoon with intense hurricane winds and precipitation affecting the immediate area. The presence of modern (bomb-carbon influenced) leaves in the coarse-grained intervals indicates that some modern organics are being deposited in the sinkhole through hurricane-induced overland washover, and/or extreme winds, but the primary mechanism for deposition is through wave-induced density and debris flows (Figure 6).

During a hurricane, wave base would increase causing bottom turbulence and resuspension of sediment (muds, shells, and pebbles) in the shallow periphery of Laguna Chumkopó. As wave climate increased, erosion and margin failures of sediment outcrops around the edge of the sinkhole would cause multiple types of debris or concentrated density flows (Mulder and Alexander, 2001). This sediment includes coarser sediment, mostly shells as described from CKC2, which flow downslope reaching the ledge of the hourglass geometry of the deep sinkhole. Once the sediment reaches the overhang, it settles through the water column to the sinkhole floor producing graded fining upward sequences of sediment. The lack of sedimentary structures in each of the event layers provides further evidence of suspension deposition (Spiske and Jaffe, 2009). Upon reaching the bottom of the sinkhole, sediment may move further downslope into the central portion of the sinkhole through density currents (Figure 6). Several of these debris or density-flow events are found in the PSDs of core CKC1. The lower unit has three events (~4–5-cm thick), while the upper unit has several small events (~4–5-cm thick) followed by a large one (~15-cm thick). This progression of coarse units and their increasing mean particle size follows expected deposition during the setup, peak, and waning phases of a hurricane with the failure events increasing in size and frequency at the peak of the storm (Spiske and Jaffe, 2009).

The location of the failures and the subsequent movement of sediment downslope into the sinkhole may also vary with basin physiography. Small mounds of sediment, 1.5 m in diameter and several cm in relief, were observed on the sinkhole bottom during the coring operation (Figure 2B), indicating that failure events were concentrated at different points around the sinkhole margin. Scarps from previous failures were seen during the diver survey (Figure 2C) of the sinkhole, along with sediment transport paths downslope, but the muddy outcrops appear stable during most of the year, eroding and failing during hurricanes, as demonstrated with the dating evidence already discussed. Sediment type (*e.g.*, muddy *vs.* sandy), outcrop geometry (*e.g.*, oversteepened), and underlying limestone physiography likely play a role in the locality of

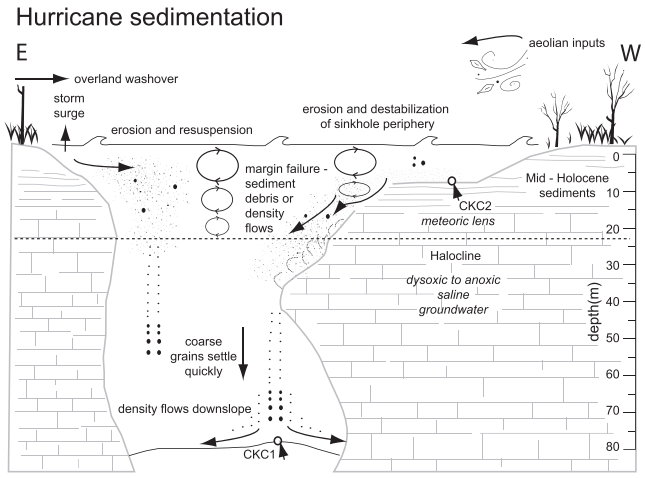

Figure 6. Depositional model illustrating possible sedimentary dynamics in Chumkopó during hurricanes.

deposition in the sinkhole. Gischler *et al.* (2008) found a lack of correspondence between storm records from their two cores from the Blue Hole in Belize proposing that smaller storms were causing limited areal deposition in the basin. Their cross-section (Figure 1; Gischler *et al.,* 2008) shows prominent piles around the periphery of the Blue Hole, which they attribute to debris from the collapsed cave roof. Based on the hourglass shape of the sinkhole, it could be that some of this is sediment accumulation from the process described for Chumkopó.

Sensitivity of Chumkopó to Hurricane Sedimentation

Overall, the sedimentary signature of a hurricane in the stratigraphic record is related to multiple factors, such as radius of maximum winds, proximity and duration of travel around a sedimentary basin of interest, the velocity of storm migration, and the pre-existing sediment available for mobilization and re-deposition. Of the 10 hurricane events that have struck the Yucatan Peninsula since 1956 AD (NOAA, 2011), none of the weaker hurricanes (categories 1–2) generated event deposits in the deep sinkhole. This suggests that wind speeds less than 48 m s^{-1} are incapable of producing the necessary wave climate and hydraulic turbulence required for sediment resuspension and slope failures into the sinkhole. In contrast, the moderate-to-intense strength hurricane events are better represented, but the overall stratigraphic record is still biased for undercounting intense hurricane events. Only two intense events (Hurricanes Gilbert 1988 and Emily 2005) have passed within a 75-km radius of Chumkopó since 1956 AD, yet only Hurricane Gilbert is recorded in the stratigraphic record. Hurricane Emily (2005) is notably absent in the stratigraphy, which was a category 4 event when it hit the coast ~65 km from Chumkopó. Hurricane Wilma also struck the Yucatan Peninsula as a category 4 event ~100 km away from Chumkopó in 2005. There is, however, no sedimentary presence in CKC1 during the last 50 years to indicate that storms beyond a 75-km radius have the capability of generating event deposits in Chumkopó. Moderate strength storms also appear undercount-

ed in the stratigraphic record, where Hurricane Beulah (1967) generated an event horizon as a category 2–3 event, yet Hurricane Roxanne (1995, category 2–3) did not. Therefore, the sinkhole is capable of recording moderate-to-intense hurricane events that make landfall within a 65-km radius of Chumkopó but does not record all events.

Sedimentary processes may be causing this lack of hurricane fidelity in the stratigraphic record in Chumkopó. The assumption that, similar to lakes, deep sinkholes archive basin-wide effects is currently unfounded and relying on one or two cores in the central areas may be inadequate. For example, short-core data in Gischler *et al.* (2008) indicates that hurricane-overwash deposits in Great Blue Hole Belize are not stratigraphically continuous between cores, and cores taken from locations close to the Blue Hole periphery contain a higher occurrence of hurricane overwash deposits *vs*. the cores from the central region of the Blue Hole (see Figure 6; Gischler *et al.,* 2008). The site geometry of Great Blue Hole, Belize, and its large reef surrounding the periphery, however, may be promoting lateral sediment sorting of hurricane transported sediments when they are deposited into the Blue Hole, as described by simple advective settling (Woodruff *et al.,* 2008). The Chumkopó sinkhole is not rimmed by a reef like the Great Blue Hole, so similar sediment-transport processes are not affecting Chumkopó; however, in both cases, the hurricane depositional record is very patchy in extent and may require multiple cores to build a complete chronology of events (Gischler *et al.,* 2008).

CONCLUSIONS

Hurricane event deposits (fining upward sequences) from Hurricanes Gilbert (1988) and Beulah (1967) deposited in a sinkhole at the bottom of Laguna Chumkopó demonstrate that inland sinkholes can record hurricane deposits. The sinkhole core spans the last 50 years, and based on a comparison with the instrumental record, intense hurricane events striking the Yucatan within a 65-km radius of Chumkopó are most likely to be recorded in the stratigraphic record. The stratigraphic record for intense hurricane events, however, was still biased for undercounting, which is similar to other coastal environments used for paleohurricane research. This is perhaps related to the location where hurricanes strike the Yucatan coast and their radius of maximum winds impacting the wave climate in Laguna Chumkopó, as both Hurricanes Gilbert and Beulah hit ~65 km to the north of Chumkopó and followed a nearly identical geographic migration route. After considering the sensitivity of Chumkopó to historic hurricane events, it appears that hurricanes of greater intensity (≥category 3) and those traveling within close proximity (75-km radius) of Chumkopó are more likely to be recorded within the sinkhole. Future research combining hurricane records from multiple cores in sinkhole basins may provide a more complete stratigraphic representation and perhaps allow assessment of hurricane strength by the extent of the deposits. Despite these limitations, deep anoxic sinkholes with long undisturbed records unaffected by storm reworking and bioturbation are a strong attractor for future hurricane research in tropical karst terrains.

ACKNOWLEDGMENTS

Fieldwork support was provided by members of CINDAQ and Global Underwater Explorers (F. Devos, C. le Malliot, D. Riordan, S. Meacham, J. Jablonski, and D. Rhea) and David Rhea for the underwater photographs. This project was funded by the National Sciences and Engineering Research Council of Canada (NSERC) awards to EGR (Discovery Grant) and PvH (Post-Doctoral Fellowship) and National Geographic Research and Exploration Grant (EGR).

LITERATURE CITED

Alverez Zarikian, C.A.; Swart, P.K.; Gifford, J.A., and Blackwelder, P.L., 2005. Holocene paleohydrology of Little Salt Spring, Florida, based on ostracod assemblages and stable isotopes. *Palaeogeography, Palaeoclimatology, Palaeoecology,* 225(1–4), 134–156.

Beddows, P.A., 2004. Groundwater Hydrology of a Coastal Conduit Carbonate Aquifer: Caribbean Coast of the Yucatan Peninsula, Mexico. Bristol, United Kingdom: University of Bristol, Ph.D. thesis, 303p.

Beddows, P.A., 2005. Density stratified groundwater circulation on the Caribbean coast of Yucatan Peninsula, Mexico. *In:* Martin, J.B.; Wicks, C.M., and Sasowsky, I.D. (eds.), *Hydrogeology and Biology of Post-Paleozoic Carbonate Aquifers*. Leesburg, Virginia: Karst Waters, pp. 129–134.

Beddows, P.A.; Smart, P.L.; Whitaker, F.F., and Smith, S., 2007. Decoupled fresh-saline groundwater circulation of a coastal carbonate aquifer: spatial patterns of temperature and specific conductivity. *Journal of Hydrology*, 346, 18–22.

Beierle, B.D.; Lamoureux, S.F.; Cockburn, J.M.H., and Spooner, I., 2002. A new method for visualizing sediment particle size distribution. *Journal of Paleolimnology*, 27(2), 279–283.

Bernhardt, C.E.; Willard, D.A.; Landacre, B., and Gifford, J., 2010. Vegetation changes during the last deglacial and early Holocene: A record from Little Salt Spring Florida. *In: American Geophysical Union Fall Meeting* (San Francisco, California, USA), Abstract no. PP41B-1635.

Blaauw, M., 2010. Methods and code for 'classical' age-modeling of radiocarbon sequences. *Quaternary Geochronology*, 5, 512–518.

Boldt, K.V.; Lane, P.; Woodruff, J.D., and Donnelly, J.P., 2010. Calibrating a sedimentary record of overwash from Southeastern New England using modeled historic hurricane surges. *Marine Geology*, 275, 127–139.

Boose, E. R.; Foster, D.R.; Barker Plotkin, A., and Hall, B., 2003. Geographical and historical variation in hurricanes across the Yucatan Peninsula. *In:* Gómez-Pompa, A.; Allen, M.F.; Fedick, S.L., and Jiménez J.J. (eds.), *Lowland Maya Area: Three Millennia at the Human-Wildland Interface*. New York: Haworth, pp. 495–516.

Castañeda-Moya, E.; Twilley, R.R.; Rivera-Monroy, V.H.; Zhang, K.; Davis, S.E., and Ross, M., 2010. Sediment and nutrient deposition associated with Hurricane Wilma in Mangroves of Florida Coastal Everglades. *Estuaries and Coasts,* 33(1), 45–58.

Diez, J.J.; Esteban, M.D., and Paz, R.M., 2009. Cancun-Nizuc Coastal Barrier. *Journal of Coastal Research*, 25(1), 57–68.

Dill, R.F.; Land, L.S.; Mack, L.E., and Schwarcz, H.P., 1988. A submerged stalactite from Belize: petrography, geochemistry, and geochronology of massive marine cementation. *Carbonites and Evaporites,* 13(2), 189–197.

Donato, S.V.; Reinhardt, E.G.; Boyce, J.I.; Pilarczyk, J.E., and Jupp, B.P., 2009. Particle-size distribution of inferred tsunami deposits in Sur Lagoon, Sultanate of Oman. *Marine Geology*, 257, 54–64.

Donnelly, J.P.; Smith Bryant, S.; Butler, J.; Dowling, J.; Fan, L.; Hausmann, N.; Newby, P.; Shuman, B.; Stern, J.; Westhover, K., and Webb, T.I., 2001. 700 yr sedimentary record of intense hurricane landfalls in southern New England. *Geological Society of America Bulletin*, 113(6), 715–727.

Donnelly, J.P., and Woodruff, J.D., 2007. Intense hurricane activity over the past 5,000 years controlled by El Niño and the West African Monsoon. *Nature,* 447, 465–468.

Gabriel, J.J.; Reinhardt, E.G.; Peros, M.C.; Davidson, D.E.; van Hengstum, P.J., and Beddows, P.A., 2009. Palaeoenvironmental evolution of Cenote Aktun Ha (Carwash) on the Yucatan Peninsula, Mexico and its response to Holocene sea-level rise. *Journal of Paleolimnology,* 42(2), 199–213.

Gischler, E. and Hudson, J.H., 2004. Holocene development of the Belize Barrier Reef. *Sedimentary Geology,* 164(3–4), 223–236.

Gischler, E.; Shinn, E.A.; Oschmann, W.; Fiebig, J., and Buster, N.A., 2008. A 1500-year Holocene Caribbean climate archive from the Blue Hole, Lighthouse Reef, Belize. *Journal of Coastal Research*, 24(6), 1495–1505.

Heiri, O.; Lotter, A.F., and Lemcke, G., 2001. Loss on ignition as a method for estimating organic and carbonate content in sediments: reproducibility and comparability of results. *Journal of Paleolimnology,* 25, 101–110.

Horton, B.P.; Rossi, V., and Hawkes, A.D., 2009. The sedimentary record of the 2005 hurricane season from the Mississippi and Alabama coastlines. *Quaternary International,* 195(1–2), 15–30.

Hua, Q. and Barbetti, M., 2004. Review of tropospheric bomb C-14 data for carbon cycle modeling and age calibration purposes. *Radiocarbon*, 46(3), 1273–1298.

Knutson, T.R.; McBride, J.L.; Chan, J.; Emmanuel, K.; Holland, G.; Landsea, C.; Held, I.; Kossin, J.P.; Srivastava, A.K., and Sugi, M., 2010. Tropical cyclones and climate changes. *Nature Geoscience*, 3, 157–163.

Lamb, A.L.; Wilson, G.P., and Leng, M.J., 2006. A review of coastal paleoclimate and relative sea-level reconstructions using δ13C and C/N ratios in organic material. *Earth Science Reviews,* 75(1–4), 29–57.

Lane, P.; Donnelly, J.P.; Woodruff, J.D., and Hawkes, A.D., 2011. A decadally-resolved paleohurricane record archived in the late Holocene sediments of a Florida sinkhole. *Marine Geology,* 287(1–4), 14–30.

Liu, K.-b., and Fearn, M.L., 1993. Lake-sediment record of late Holocene hurricane activities from coastal Alabama. *Geology,* 21(9), 793–796.

Liu, K.-b., and Fearn, M.L., 2000. Reconstruction of prehistoric landfall frequencies of catastrophic hurricanes in NW Florida from lake sediment records. *Quaternary Research*, 52(2), 238–245.

Marshall, W.A.; Gehrels, W.R.; Garnett, M.H.; Freeman, S.P.H.T.; Maden, C., and Xu, S., 2007. The use of 'bomb spike' calibration and high-precision AMS 14C analyses to date salt-marsh sediments deposited during the past three centuries. *Quaternary Research*, 68(3), 325–337.

Meacham, S.S., 2012. Using Landsat 5 TM Data to Identify and Map Areas of Mangrove in Tulum, Quintana Roo, Mexico. Durham, New Hampshire: University of New Hampshire, Master's thesis, 192p.

Meyer-Arendt, M.J., 1991. Hurricane Gilbert: the storm of the century. *GeoJournal,* 23(4), 323–325.

Monarstersky, R., 1988. Focusing on Gilbert's extra eye (Hurricane Gilbert). *Science News,* 134(13), 1–2.

Moore, Y.H.; Stoessell, R.K., and Easley, D.H., 1992. Fresh-water/sea-water relationship within a ground-water flow system, northeastern coast of the Yucatan Peninsula. *Ground Water*, 30(3), 343–350.

Morton, R.A. and Sallenger, A.H., Jr., 2003. Morphological impacts of extreme storms on sandy beaches and barriers. *Marine Geology*, 19(3), 560–573.

Mulder, T. and Alexander J., 2001.The physical character of subaqueous sedimentary density flows and their deposits. *Sedimentology*, 48(2), 269–299.

Mylroie, J.E.; Carew, J.L., and Moore, A.I., 1995. Blue holes: definitions and genesis. *Carbonates and Evaporites*, 10(2), 225–233.

National Oceanic and Atmospheric Administration (NOAA), 2010. http://www.nhc.noaa.gov.

NOAA: Hurricane Research Division Re-Analysis Project, 2011. http://www.aoml.noaa.gov/hrd/hurdat/Data_Storm.html.

Nyberg, J.; Malmgren, B.A.; Winter, A.; Jury, M.R.; Kilbourne, K.H., and Quinn, T.M., 2007. Low Atlantic hurricane activity in the 1970s and 1980s compared to the past 270 years. *Nature*, 477, 698–701.

Nyman, J.A.; Crozier, C.R., and DeLaune, R.D., 1995. Roles and patterns of hurricane sedimentation in an estuarine marsh landscape. *Estuarine, Coastal, and Shelf Science,* 40(6), 665–679.

Parsons, M.L., 1998. Salt marsh sedimentary record of the landfall of Hurricane Andrew on the Louisiana coast: diatoms and other paleoindicators. *Journal of Coastal Research*, 14(3), 939–950.

Pennington, W.; Cambray, R.S., and Fisher, E.M., 1973. Observations on lake sediments using fallout ^{137}Cs as a tracer. *Nature*, 242, 324–326.

Reese, C.A.; Strange, T.P.; Lynch, W.D., and Liu, K., 2008. Geologic evidence of Hurricane Katrina recovered from the Pearl River Marsh, MS/LA. *Journal of Coastal Research*, 24(6), 1601–1607.

Reimer, P.J.; Baillie, M.G.L.; Bard, E.; Bayliss, A.; Beck, J.W.; Blackwell, P.G.; Ramsey, C.B.; Buck, C.E.; Burr, G.S.; Edwards, R.L.; Freidrich, M.; Groots, P.M.; Guilderson, T.P.; Hajdas, I.; Heaton, T.J.; Hogg, A.G.; Hughen, K.A.; Kaiser, K.F.; Kromer, B.; McCormac, F.G.; Manning, S.W.; Reimer, R.W.; Richards, D.A.; Southon, J.R.; Talamo, S.; Turney, C.S.M.; van der Plicht, J., and Weyhenmeyer, C.E., 2009. IntCal09 and Marine09 radiocarbon age calibration curves, 0–50,000 years Cal BP. *Radiocarbon*, 51(4), 1111–1150.

Reimer, P.J.; Brown, T.A., and Reimer, R.W., 2004. Discussion: reporting and calibration of post-bomb 14C data. *Radiocarbon*, 46(3), 1299–1304.

Reinhardt, E.G.; Nairn, R.B., and Lopez, G., 2010. Recovery estimates for the Rio Cruces after the May 1960 Chilean earthquake. *Marine Geology,* 269, 18–33.

Ritchie, J.C. and McHenry, J.R., 1990. Application of radioactive fallout Cesium-137 for measuring soil erosion and sediment accumulation rates and patterns: a review. *Journal of Environmental Quality,* 19(2), 215–233.

Robbins, L.L.; Tao, Y., and Evans, C.A., 1997. Temporal and spatial distribution of whitings on Great Bahama Bank and a new lime budget. *Geology*, 25(10), 947–950.

Schwabe, S. and Herbert, R.A., 2004. Black holes of the Bahamas: what they are and why they are black. *Quaternary International*, 121(1), 3–11.

Shinn, E.A.; Reich, C.D.; Locker, S.D., and Hine, A.C., 1996. A giant sediment trap in the Florida Keys. *Journal of Coastal Research*, 12(4), 953–959.

Smart, P.L.; Beddows, P.A.; Coke, J.; Doerr, S.; Smith, S., and Whitaker, F.F., 2006. Cave development on the Caribbean coast of the Yucatan Peninsula, Quintana Roo, Mexico, *In:* Harmon, R.S. and Wicks, C.M. (eds.), *Perspectives on Karst Geomorphology, Hydrology, and Geochemistry: A Tribute Volume to* Derek C. Ford and William B. *White*, Geological Society of America, Special Paper 404, pp. 105–128.

Spiske, M. and Jaffe, B., 2009. Sedimentology and hydrodynamic implications of a coarse-grained hurricane sequence in a carbonate reef setting. *Geology,* 37(9), 839–842.

Steadman, D.W.; Franz, R.; Morgan, G.S.; Albury, N.A.; Kakuk, B.; Broad, K.; Franz, S.E.; Tinker, K.; Pateman, M.P.; Lott, T.A.; Jarzen, D.M., and Dilcher, D.L., 2007. Exceptionally well preserved late Quaternary plant and vertebrate fossils from a blue hole on Abaco, The Bahamas. *Proceedings of the National Academy of Sciences,* 104(50), 19897–19902.

Surić, M.; Juračić, M.; Horvatinčić, N., and Bronić, I.K., 2005. Late-Pleistocene-Holocene sea-level rise and the pattern of coastal karst inundation: records from submerged speleothems along the Eastern Adriatic Coast (Croatia). *Marine Geology,* 214(1–3), 163–175.

van Hengstum, P.J. and Scott, D.B., 2012. Sea-level rise and coastal circulation controlled Holocene groundwater development in Bermuda and caused a meteoric lens to collapse 1600 years ago. *Marine Micropaleontology*, 90–91, 29–43.

van Hengstum, P.J.; Reinhardt, E.G.; Boyce, J.I., and Clark, C., 2007. Changing sedimentation patterns due to historical land-use change in Frenchman's Bay, Pickering, Canada: evidence from high-resolution textural analysis. *Journal of Paleolimnology,* 37(4), 603–618.

van Hengstum, P.J.; Scott, D.B.; Gröcke, D.R., and Charette, M.A., 2011. Sea level controls sedimentation and environments in coastal caves and sinkholes. *Marine Geology*, 286(1–4), 35–50.

Webster, P.J.; Holland, G.J.; Curry, J.A., and Chang, H.R., 2005. Changes in tropical cyclone number, duration, and intensity in a warming environment. *Science,* 309(5742), 1844–1846.

Weidie, A.E., 1985. Geology of the Yucatan Platform. *In:* Ward, W.C.; Weidie, A.E., and Back, W. (eds.), *Geology and Hydrogeology of the Yucatan and Quaternary Geology of the Northeastern Yucatan Peninsula*. New Orleans: Geological Society, pp. 1–9.

Whitaker, F.F. and Smart, P.L., 1990. Active circulation of saline ground waters in carbonate platforms: evidence from the Great Bahama Bank. *Geology*, 18(3), 200–203.

Woodruff, J.D.; Donnelly, J.P.; Mohrig, D., and Geyer, W.R., 2008. Reconstruction relative flooding intensities responsible for hurricane induced deposits from Laguna Playa Grande, Vieques, Puerto Rico. *Geology,* 36, 391–394.

Wright, V.P. and Burchette, T.P., 1996. Shallow-water carbonate environments. *In:* Reading, H.G. (ed.), *Sedimentary Environments: Processes, Facies and Stratigraphy*. Cambridge, Massachusetts: Blackwell Science, pp. 325–330.